Four-Element Compact Planar Antenna Array for Robust Satellite Navigation Systems

S. Irteza[1], E. Schäfer[2], M. Sgammini[3], R. Stephan[1], M. A. Hein[1]
[1] RF and Microwave Laboratory, Ilmenau University of Technology, Germany
[2] Institut für Mikroelektronik- und Mechatronik-Systeme gemeinnützige GmbH, Germany
[3] German Aerospace Center (DLR), Institute for Communication and Navigation, Germany
Email: safwat-irteza.butt@tu-ilmenau.de

***Abstract*—In this paper, we present a four-element compact planar antenna array for global navigation satellite systems. The array is designed for the 1575.42 MHz (L1 band) frequency having an inter-element separation of $d = \lambda/4$. In order to compensate mutual coupling and mismatching, a specifically designed decoupling and matching network has been integrated into the array. We investigate the resulting antenna performance, such as axial-ratio bandwidth, and realized gain, as referred to the decoupling and matching network input ports. Furthermore, we present a receiver model to characterize the equivalent spatial carrier-to-interference plus noise ratio of the antenna array, decoupling and matching network, and low-noise amplifier, using a conventional null-constraint beamformer.**

***Index Terms*—compact, planar antenna array, navigation systems, mutual coupling, decoupling and matching network, carrier-to-interference plus noise ratio**

I. INTRODUCTION

Since few years, the use of multi-element antenna arrays in global positioning navigation systems (GNSS) has been proposed, to provide robustness against in-band interference and multi-path propagation. This approach provides the opportunity of using sophisticated beamforming techniques to null-out the unwanted signals. However, the overall physical size is restricted by the inter-element separation of $d = \lambda/2$, i.e., about 10 cm, to minimize the detrimental mutual coupling effects.

Reduced inter-element separation, i.e., $d < \lambda/2$, inflicts strong mutual coupling between the elements, and degrades the radiation performance of the antenna severely, particularly for higher order modes. As discussed in [1], this degradation results in smaller eigenvalues for the radiation covariance matrix. Smaller eigenvalues mean lower carrier-to-interference-plus-noise ratio (CINR), which is undesirable especially for adaptive navigation systems, due to longer transient times for signal detection, nulling, and tracking. Consequently, it undermines the advantages of the usage of multi-element antenna arrays in an interference-limited scenario.

Strong mutual coupling can be mitigated using a decoupling and matching network (DMN) [1]. This will result in a partial restoration of the signal-to-noise ratio, as shown in

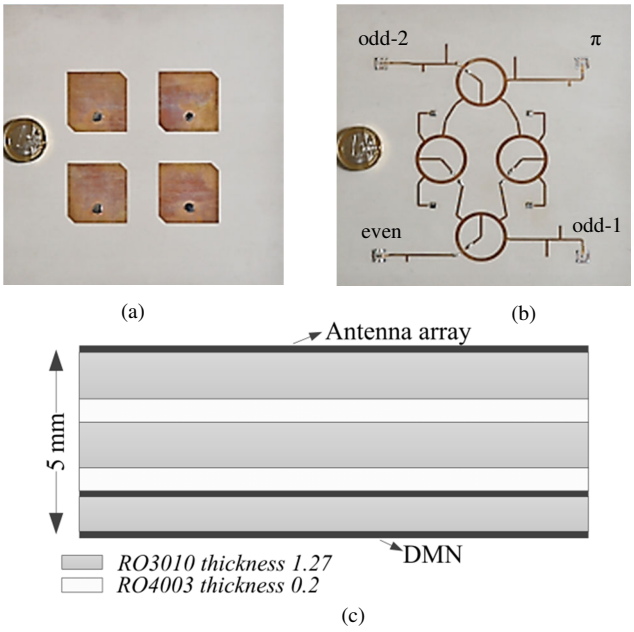

Fig. 1: (a) Top view of the GNSS antenna array designed in this work. (b) DMN with numberings indicating the respective mode excitations, bottom view of the designed GNSS antenna array. (c) Exploded view of the stacked-substrate configuration of the antenna array.

[2]. However, the analyses in the aforementioned publications lack practical implementations and assume the network to be lossless, which obviously is unrealistic. While the DMN maximizes the energy transfer from receiver to antenna, it exhibits ohmic losses. This loss of useful energy will result in increased noise, and may become dominant over the network gain when used before a low-noise amplifier in the receive path, which is typically the case. Therefore, it is important to characterize or include the network noise in order to calculate the CINR for an accurate performance assessment of the compact antenna array receivers.

The aim of this paper is to present a compact L1-band GNSS antenna array with integrated DMN, and the framework to analyze its performance using the CINR at the output of a null-constraint beamformer [3]. In this regard, Section II presents the compact L1-band GNSS integrated antenna array

978-88-907018-3-2/13 ©2013 IEEE

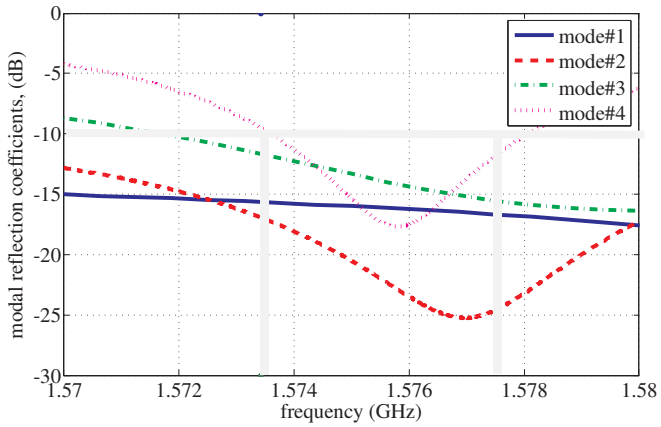

Fig. 2: Measured reflection or matching coefficients S_{ii} of the antenna array with DMN for respective modes. The highlighted lines indicate the required threshold for a L1-band navigation system, Mode#1, #2, #3, #4 indicate the even, odd 1, odd 2, and π-mode, respectively.

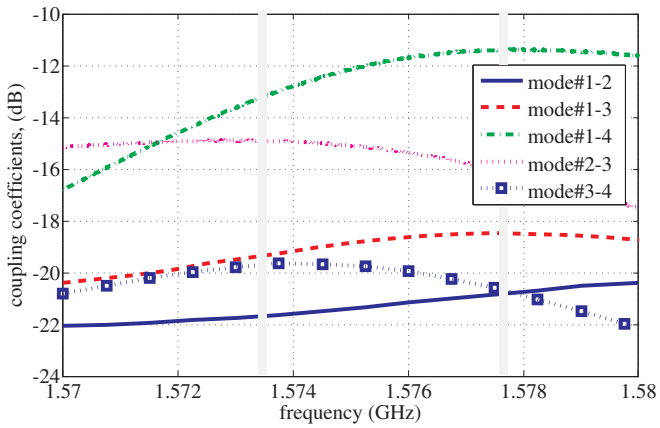

Fig. 3: Measured coupling coefficients S_{ij} of the antenna array with DMN among respective modes.

along with its noise parameters. Section III describes the formulation of equivalent CINR, and in section IV results based on CINR for with and without DMN for different interference conditions are presented. Finally, conclusions are drawn in Section V.

II. Compact L1 GNSS Antenna Array Receiver

In this section, we initially discuss the design and measured parameters of the integrated antenna array. Secondly, we define the noise-contribution parameters for the antenna array, low-noise amplifier, and beamformer. We use these parameters to analyze the equivalent carrier-to-interference-plus-noise ratio for two scenarios, with and without DMN, in the next section.

A. Antenna array

The antenna array consists of four truncated square patches as shown in Fig. 1 (a), on a substrate with a dielectric permittivity of $\varepsilon_r = 10.2$, with a thickness of $t = 2.74$ mm. The truncated square patches usually exhibit a narrow axial ratio bandwidth [4], which is enhanced by increasing the thickness of the substrate.

The radiation matrix of the antenna array is defined as $\mathbf{H}_A$, where

$$\mathbf{H}_A = \frac{1}{4\pi} \oiint \mathbf{F}(\phi,\theta)\mathbf{F}^H(\phi,\theta)\, d\Omega\,. \qquad (1)$$

The individual elements of column vector $\mathbf{F}(\phi,\theta)$ denote the normalized complex-valued realized RHCP gain pattern of the single antennas with respect to an isotropic radiator [4]. Ω denotes the solid angle, $d\Omega = \theta \cdot \sin\theta \cdot \sin\phi$.

The combined noise temperature correlation matrix of antenna array and DMN is calculated from [5]

$$\mathbf{T}_A = T_{env}\mathbf{H}_A^T + T_{amb}\left(\left(\mathbf{I} - \mathbf{S}_A\mathbf{S}_A^H\right) - \mathbf{H}_A\right)^T, \qquad (2)$$

where $\mathbf{S}_A$ denotes the S-parameter matrices of the antenna array and DMN combined. $\mathbf{T}_A$ includes noise received from the environment as well as from the antenna network, $T_{env} = 100$ K is the assumed equivalent isotropic environmental temperature for GNSS conditions; $T_{amb} = 290$ K is the ambient temperature of the antennas.

B. Decoupling and Matching network

The DMN shown in Fig. 1 (b) was designed using four 180-degrees hybrids and tuning stubs, ensuing to the eigenmode excitations mentioned in [6]. In order to minimize the losses between the network and the antenna feed-points in our design, the outputs of the DMN are directly connected to the antenna using vias. The complete substrate-stack is sketched in Fig. 1 (c). The reflection coefficients for respective modes are shown in Fig. 2. The measured values are $S_{ii} \leq -10$ dB for all radiation modes, within a bandwidth of 4 MHz centered at 1575.42 MHz (L1). Due to imperfect eigenmode decoupling using hybrids, the coupling coefficients are below −15 dB, with an exception of $S_{14} < -11$ dB, as shown in Fig. 3. This is acceptable but not ideal, and could be improved by more careful design and thinner network substrate.

The output modal RHCP radiation patterns are shown in Fig. 4 (a), along with exact simulated eigenmodes RHCP radiation patterns in Fig. 4 (b). The measured total modal efficiencies are 64%, 56%, 35%, and 28%, respectively, compared to exact eigeneffieciencies, i.e., 90%, 52%, 38%, and 10%, respectively.

The measured axial ratio for the even mode in main-lobe direction is less than 3 dB, with a bandwidth larger than 4 MHz; fulfilling the specifications for L1 signals (see Fig. 5 (a)). It is also observed that the XPD, shown in Fig. 5 (b), is considerably degraded for the higher order modes, also for the even mode at lower elevations, i.e., $\theta > 60°$. In interference limited scenario for weak navigation signals, such a shortcoming is harmful, and may not blind or null-out the interferer entirely.

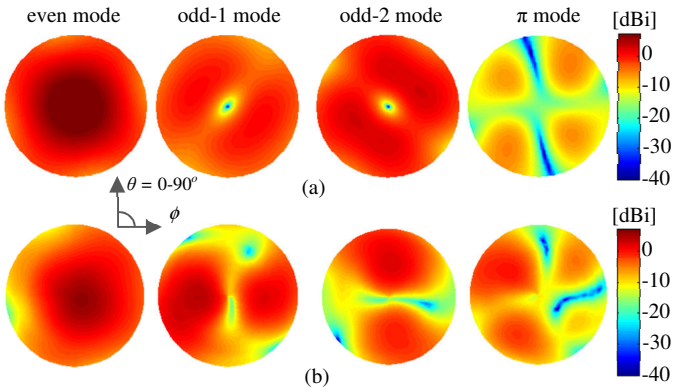

Fig. 4: (a) Exact simulated eigenmode RHCP radiation patterns (b) Measured realized gain patterns at the respective output ports of DMN. The DMN is based on the principal of eigenmode excitations, therefore each patterns represents a mode. The π mode has the minimum efficiency and a maximum gain of 0.2 dBi.

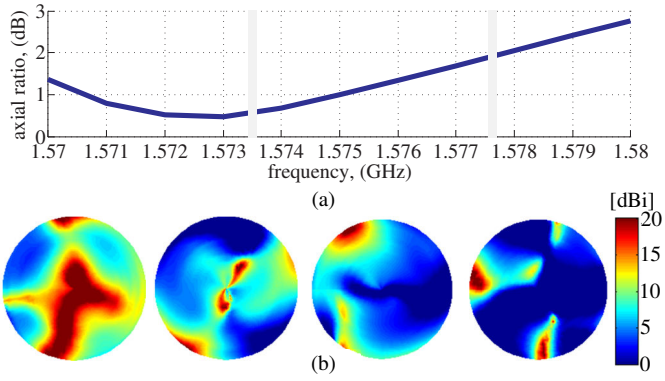

Fig. 5: (a) Measured axial ratio in main lobe direction of mode#1 vs. frequency, within the highlighted (thick vertical lines) L1 band, (b) The cross-polar discrimination (XPD), i.e., the RHCP (wanted) component minus the LHCP (unwanted) component in dB.

C. Low-noise amplifier

The signal power available from the satellites is typically about one order of magnitude below the noise level. Since the noise budget for the whole receiver chain is quite low, a low-noise amplifier is applied close to the antenna output, to attain low noise figures for the complete front-end. In addition, we also incorporate a low loss filter before the amplifier, for better out-of-band interference rejection. The measured on-board noise parameters [7] of designed amplifier are $F_{\min} = 1.66$ dB, $R_n = 8.2\ \Omega$, and $|Z_{opt}| = 29\ \Omega$. The noise contribution due to the amplifiers is calculated according to Warnick *et al.* [2]. The amplifier noise temperature correlation matrix is defined as:

$$\mathbf{T}_{\mathrm{LNA}} = \left(\mathbf{T}_{\alpha} + \mathbf{S}_{\mathrm{A}}\mathbf{T}_{\beta}\mathbf{S}_{\mathrm{A}}^{\mathrm{H}} - \mathbf{S}_{\mathrm{A}}\mathbf{T}_{\gamma} - \mathbf{T}_{\gamma}^{\mathrm{H}}\mathbf{S}_{\mathrm{A}}^{\mathrm{H}}\right), \tag{3}$$

We assume that the noise generated by one LNA is uncorrelated with all other amplifiers. Therefore, the input-referred noise correlation matrices in (3) simplify to $\mathbf{T}_\alpha = T_\alpha\mathbf{I}$, $\mathbf{T}_\beta = T_\beta\mathbf{I}$, and $\mathbf{T}_\gamma = T_\gamma\mathbf{I}$, in which T_α, T_β, and T_γ are calculated from the measured noise parameters $F_{\min}$, R_n, and Z_{opt} [7].

D. Beamformer

To assess the equivalent CINR, a modified version of the well-known null-constraint beamformer, differing in the selection of the zero-order constrains is considered. The optimum weighting coefficients are obtained using:

$$\mathbf{w} = \mathbf{w}_d^H - (\mathbf{w}_d^H\mathbf{w}_I(\mathbf{w}_i^H\mathbf{w}_I)^{-1}\mathbf{w}_i^H), \tag{4}$$

where $\mathbf{w}_d$ is the eigenmode vector response at the desired direction of the signal, $\mathbf{w}_I$ is defined as the null-constraint matrix for the unwanted direction of interferers, with columns representing the interferer. Non-linear effects due to analog-to-digital conversions are not considered for further discussion.

III. Carrier-to-Interference-plus-Noise Ratio

The receiver model of our approach is depicted in Fig. 6. The equivalent available carrier power is calculated from

$$C(\phi,\theta) = C_{\mathrm{sat}}\mathbf{w}^{\mathrm{H}}\mathbf{F}(\phi,\theta)\mathbf{F}^{\mathrm{H}}(\phi,\theta)\mathbf{w}, \tag{5}$$

C_{sat} is the power received with an ideal RHCP isotropic antenna. We derive the noise power spectral density from the equivalent system noise temperature T_{sys}, referred to the LNA inputs:

$$N_0 = k_{\mathrm{B}}T_{\mathrm{sys}} = k_{\mathrm{B}}\underbrace{\mathbf{w}^{\mathrm{H}}\mathbf{T}_{\mathrm{A}}\mathbf{w}}_{T_{\mathrm{A}}} + k_{\mathrm{B}}\underbrace{\frac{\mathbf{w}^{\mathrm{H}}\mathbf{T}_{\mathrm{LNA}}\mathbf{w}}{\mathbf{w}^{\mathrm{H}}\left(\mathbf{I}-\mathbf{S}_{\mathrm{A}}\mathbf{S}_{\mathrm{A}}^{\mathrm{H}}\right)\mathbf{w}}}_{T_{\mathrm{LNA}}}, \tag{6}$$

$\mathbf{T}_{\mathrm{A}}$ and $\mathbf{T}_{\mathrm{LNA}}$ denote the noise temperature correlation matrices of the antenna array and the LNA, respectively. k_{B} is the Boltzmann constant, which is 1.38×10^{-23} JK^{-1}. The equivalent available interferer power is defined as:

$$I_{\mathrm{int}}(\phi,\theta) = I_{\mathrm{int}}\mathbf{w}^{\mathrm{H}}\mathbf{F}(\phi,\theta)\mathbf{F}^{\mathrm{H}}(\phi,\theta)\mathbf{w}, \tag{7}$$

where I_{int} is the power received from the interferer by an ideal RHCP isotropic antenna. This leads to the equivalent CINR,

$$CINR(\phi,\theta) = \frac{C(\phi,\theta)}{N_0 + \sum_i I_{\mathrm{int}_i}(\phi,\theta)}. \tag{8}$$

IV. Results and Discussion

To evaluate the antenna performance for GNSS applications, C_{sat} is considered to be −157 dBW [8]. Then, the desired signal direction-of-arrival (DoA) is steered across the upper hemisphere, with fixed directions of interferers. The weighting-coefficient vector $\mathbf{w}$ for every DoA is applied to eqs. (5) - (7), in the end the $CINR(\phi, \theta)$ using eq. (8) is calculated for the respective DoA. It is essential to mention that in a no-interferer situation, the use of a DMN is not necessary due to additional losses, unless lower elevation, i.e., $\theta > 60^{\circ}$ signals are to be exploited, which is normally not the case for navigation systems. Now, we consider different scenarios for evaluation of antenna arrays with and without DMN, respectively. In these

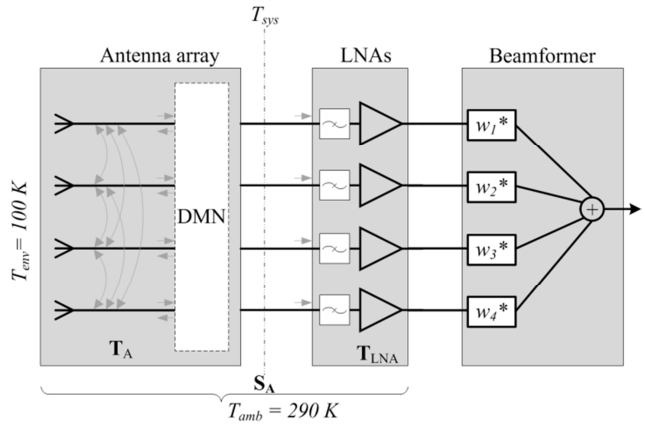

Fig. 6: Receiver model: DMN denotes the decoupling and matching network. $\mathbf{S}_A$ indicates the combined S-parameter matrix of antenna array and DMN. The conventional configuration excludes the DMN, and then $\mathbf{S}_A$ reduces to the S-parameter matrix of the antenna array. $\mathbf{T}_A$ and $\mathbf{T}_{LNA}$ are the noise correlation matrices of antenna array and low noise amplifier, respectively. Equivalent CINR is obtained after the null-constraint beamformer.

scenarios, the equivalent isotropic radiated power of each interferer is fixed to 10 dBW.

A. *Single interferer*

A single interferer, fixed at $\phi_i = 90°$, $\theta_i = 60°$ is projected upon the antenna array. The resulting CINR for the cases with and without DMN is shown as a polar map in Fig. 7. Both cases can achieve a null-constraint perfectly, but with DMN, lower elevations and signals close to the direction of interferer directions have increased CINR, as compared to the without DMN. The ϕ-cut with $\theta_i = 60°$ is shown in Fig. 8 (a). Both cases display similar CINR, while the presence of DMN leads to a marginal gain at certain directions. In a statistical approach, the empirical cumulative distribution function of $CINR(\phi, \theta)$ is shown in Fig. 9. It can be seen that for a given threshold CINR, the outage probability is higher without DMN, which indicates a poor diversity performance.

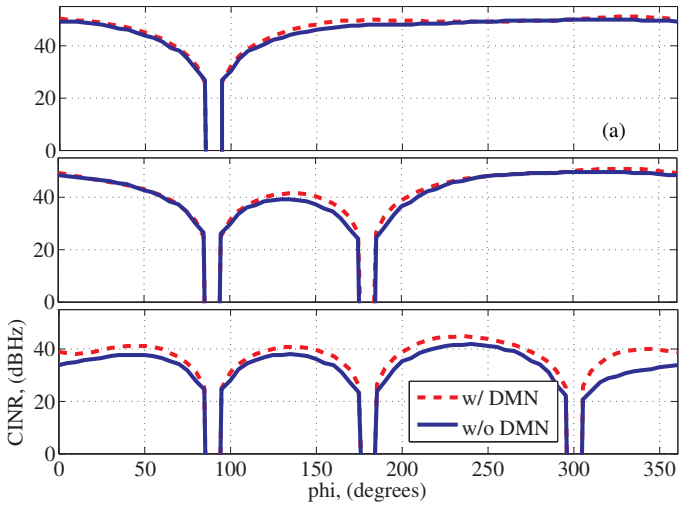

Fig. 8: ϕ-cut at $\theta = 60°$ for the calculated CINR (dBHz) (a) for one interferer, (b) two interferers, and (c) three interferers.

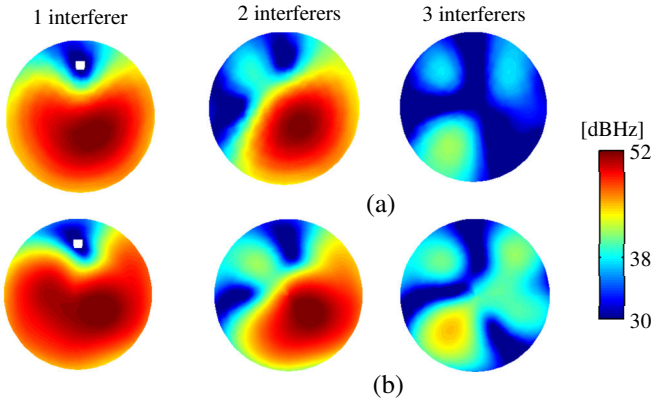

Fig. 7: *CINR* (ϕ, θ) with I_{int} = 10 dBW fixed at $\phi_i = 90°$, $\theta_i = 60°$ for one interferer, $\phi_i = 90°$, 180°, $\theta_i = 60°$ for two interferers, and $\phi_i = 90°$, 180°, 360°, $\theta_i = 60°$ for three interferers. (a) Simulated antenna array without DMN. (b) Measured antenna array with DMN.

B. *Two interferers*

Now, we study the illumination by two interferers, fixed at $\phi_i = 90°$, 180°, $\theta_i = 60°$. It is evident from Fig. 7, that lower elevations and directions close to the interferers, again, take advantage of the DMN and show better CINR performance. In the ϕ-cut higher CINR performance is achieved around the second interferer due to the increased matching gain in odd-2 mode with DMN. However, the outage probability for a given threshold CINR has no significant advantage for this case, which may be due to the choice of null-constraints for the beamformer. Nulling depth is below -150 dBHz for with and without DMN.

C. *Three interferers*

The maximum number of interferers that can be null-out using a four-element antenna array is three. It is the worst-case as it mainly relies on the use of the π-mode, which is most strongly affected by mutual coupling. The interferers are fixed at $\phi_i = 90°$, 180°, 360°, $\theta_i = 60°$ directions. The CINR polar plots shown in Fig. 7 clearly indicate the superior performance of the case with DMN. The CINR increases by at least 3 dB in all directions with the employment of the DMN, which is

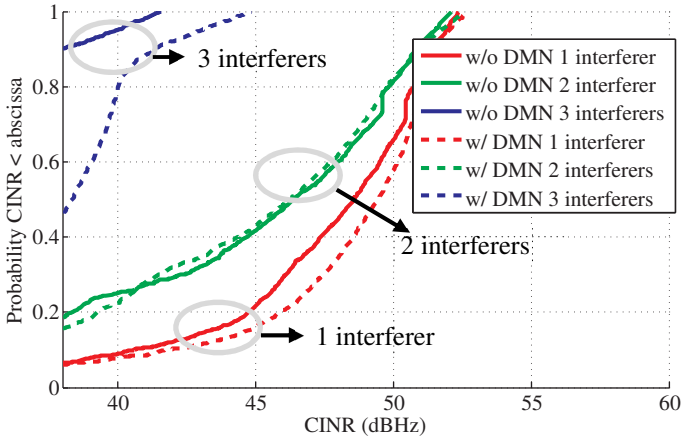

Fig. 9: Empirical cumulative distribution function (CDF) for calculated *CINR* (ϕ, θ) for different numbers of interferers, with and without DMN.

significant for navigation signals. A nulling depth less than -150 dBHz is achieved for all the three interferers with and without DMN. In the ϕ-cut, all azimuth directions show better CINR with DMN, in contrast to the previous scenarios where performance gain was limited to certain directions. In terms of outage probability, considering a threshold of 38 dBHz [9], it drops from 90% to 50%, which suggests the use of DMN a must in the interference-limited scenario for compact antenna arrays.

V. CONCLUSIONS

A GNSS four-element compact antenna array was designed, fabricated and analyzed. We defined the noise temperature correlation matrices for the integrated antenna array and low-noise amplifier, required to analyze the CINR performance using measured farfield radiation patterns and scattering parameters. In addition, we developed a receiver model for calculation of the equivalent CINR as a figure-of-merit in GNSS applications. It has been shown that in order to achieve robustness or higher CINR with such a compact antenna array, it is *necessary to employ a DMN* between the antenna and first LNA stage, especially for the case of the maximum number of interferes. As future work, the polarization impurity will also be considered for CINR calculations.

ACKNOWLEDGMENT

We gratefully acknowledge M. Huhn and M. Zocher for their technical assistance. The authors would also like to thank Dr. A. Dreher and Dr. C. Volmer for their valuable suggestions and discussions in this work. This work was supported by the German Aerospace Center (DLR) on behalf of the German Federal Ministry of Economics and Technology under Grant 50NA1007.

REFERENCES

[1] C. Volmer, J. Weber, R. Stephan, K. Blau, and M. A. Hein, "An Eigen-Analysis of Compact Antenna Arrays and Its Application to Port Decoupling," *IEEE Trans. on Ant. and Prop.*, vol. 56, no. 2, pp. 360-370, Feb. 2008.

[2] K. F. Warnick and M. A. Jensen "Optimal Noise Matching for Mutually Coupled Arrays," *IEEE Trans. on Ant. and Prop.*, vol. 55, no. 6, pp. 1726-1731, Jun. 2007.

[3] H.L. Van Trees, "Optimum Array Processing - Part IV of Detection, Estimation and Modulation Theory," John Wiley & Sons Inc., New York, 2002.

[4] C. A. Balanis, "Antenna Theory: Analysis and Design," 2nd ed. New York: John Wiley & Sons,Inc., 1997.

[5] S. Irteza et al., "Noise Characterization of a Multi-Channel Receiver Using a Small Antenna Array with Full Diversity for Robust Satellite Navigation," IEEE International Conference on Wireless Information Technology and Systems (ICWITS), Maui (HI), USA, Nov. 2012.

[6] C. Volmer, "Compact Antenna Arrays in Mobile Communications: A Quantitative Analysis of Radiator Coupling," *Ilmenau: Univ.-Verl. Ilmenau*, 2010. - XV, 250 p. ISBN 978-3-939473-71-8.

[7] J. Engberg and T. Larsen, "Noise Theory of Linear and Nonlinear Circuits," Chichester: J. Wiley & Sons, 1995.(2010, Sep.).

[8] Galileo OS SIS ICD. [Online]. Available: http://ec.europa.eu/-enterprise/policies/satnav/galileo/files/galileo-os-sis-icd-issue1-revision1_en.pdf

[9] M. V. T. Heckler, M. Cuntz, A. Konovaltsev, L. A. Greda, and M. Meurer, "Development of Robust Safety-of-Life Navigation Receivers at the German Aerospace Center (DLR)," *IEEE MTT-S Int. Microwave Symp. Dig.* pp. 85-88, May 2010.